Fungal Genetics and Biology 147 (2021) 103507

Contents lists available at ScienceDirect

Fungal Genetics and Biology

journal homepage: www.elsevier.com/locate/yfgbi

Targeted disruption of *hir1* alters the transcriptional expression pattern of putative lignocellulolytic genes in the white-rot fungus *Pleurotus ostreatus*

Hongli Wu, Takehito Nakazawa *, Ryota Morimoto, Shivani, Masahiro Sakamoto, Yoichi Honda

Graduate School of Agriculture, Kyoto University, Sakyo-ku, Kyoto 606-8502, Japan

ARTICLE INFO

Keywords:
White rot
Basidiomycete
Mutant
Histone modification
Wood degradation

ABSTRACT

Pleurotus ostreatus is frequently used in molecular genetics and genomic studies on white-rot fungi because various molecular genetic tools and relatively well-annotated genome databases are available. To explore the molecular mechanisms underlying wood lignin degradation by *P. ostreatus*, we performed mutational analysis of a newly isolated mutant UVRM28 that exhibits decreased lignin-degrading ability on the beech wood sawdust medium. We identified that a mutation in the *hir1* gene encoding a putative histone chaperone, which probably plays an important role in DNA replication-independent nucleosome assembly, is responsible for the mutant phenotype. The expression pattern of ligninolytic genes was altered in *hir1* disruptants. The most highly expressed gene *vp2* was significantly inactivated, whereas the expression of *vp1* was remarkably upregulated (300–400 fold) at the transcription level. Conversely, many cellulolytic and xylanolytic genes were upregulated in *hir1* disruptants. Chromatin immunoprecipitation analysis suggested that the histone modification status was altered in the 5′-upstream regions of some of the up- and down-regulated lignocellulolytic genes in *hir1* disruptants compared with that in the 20b strain. Hence, our data provide new insights into the regulatory mechanisms of lignocellulolytic genes in *P. ostreatus*.

1. Introduction

Wood-decaying fungi are considered as major degraders of wood cell wall, which is composed primarily of polysaccharides (cellulose and hemicellulose) and aromatic heteropolymers (lignin) (Blanchette, 1991; Sánchez, 2009; Bugg et al., 2011). Most of the wood-decaying fungi belong to the class *Agaricomycetes* and are typically divided into two types based on their decay patterns: white-rot (Floudas et al., 2012) and brown-rot fungi (Martinez et al., 2009). Although many microbes as well as wood-decaying fungi utilize the polysaccharides present in wood biomass as carbon sources (Cragg et al., 2015; Wei et al., 2009), only white-rot fungi can efficiently degrade the lignin.

White-rot fungi display lignocellulose degradation ability by producing various hydrolytic enzymes, including cellulolytic, xylanolytic, and pectinolytic enzymes, as well as oxidative enzymes, which function coordinately to decompose lignocellulose (Floudas et al., 2012; Rytioja et al., 2014). Most of these enzymes have been characterized in biochemical studies (Lundell et al., 2010; Manavalan et al., 2015) and classified into carbohydrate-active enzymes (CAZymes) (Lombard et al., 2013). There is a total of six enzyme classes currently covered by CAZymes, namely, glycoside hydrolases (GHs), carbohydrate esterases (CEs), carbohydrate-binding modules (CBMs), glycosyl transferases (GTs), polysaccharide lyases (PLs), and auxiliary activities (AAs). Copy numbers of genes encoding CAZymes are abundant in white-rot fungi (Floudas et al., 2012), especially those of genes encoding copper-dependent oxidative enzymes belonging to GH61, which act on crystalline cellulose; and fungal class II peroxidases and multicopper oxidases, which are recognized as initial lignin degraders. Genetic transformation systems have been developed for several species of white-rot fungi, followed by molecular genetic studies on lignin degradation (Honda et al., 2000; Bartholomew et al., 2001; Tsukamoto et al., 2003; Sharma et al., 2006). In particular, reliable and efficient genetic transformation using various antibiotic resistance genes has been reported in *Pleurotus ostreatus* (Honda et al., 2000; Salame et al., 2012; Matsunaga et al., 2017). Efficient gene targeting via homologous recombination was also demonstrated in this fungus (Salame et al., 2012). Single-gene disruptants of *mnp* and *vp* genes were previously generated and their phenotypes were characterized (Salame et al., 2012; 2013; 2014). These findings enabled further comprehensive analyses of ligninolytic systems in *P. ostreatus* and provide a basic foundation for

* Corresponding author at: Graduate School of Agriculture, Kyoto University, Oiwakecho, Kitashirakawa, Sakyo-ku, Kyoto 606-8502, Japan.
E-mail address: tnakazaw@kais.kyoto-u.ac.jp (T. Nakazawa).

https://doi.org/10.1016/j.fgb.2020.103507
Received 11 June 2020; Received in revised form 28 November 2020; Accepted 22 December 2020
Available online 28 December 2020

exploring the transcriptional regulation of lignocellulolytic genes in white-rot fungi.

The transcriptional regulatory mechanisms of cellulolytic and xylanolytic genes, which mainly involve a transcription factor *cre1* that mediates carbon catabolite repression, have been extensively studied in some ascomycete filamentous fungi (Strauss et al., 1995; van Peij et al., 1998; Portnoy et al., 2011; Derntl et al., 2013). In the white-rot agaricomycete *Ganoderma lucidum*, *creA* was also shown to be repressed by the activation of a gene encoding sucrose-nonfermenting serine-threonine protein kinase 1 (Snf1) when grown on a liquid medium, which may result in increased cellulase production (Hu et al., 2020). Yoav et al. (2018) reported that disruption and overexpression of *cre1* enhanced and reduced cellulolytic activity in the liquid medium containing wheat straw in *P. ostreatus*, respectively. In addition to the affection caused by the transcription factor *cre1*, transcriptional expression of cellulolytic genes were also shown to differ depending on the growth period and different substrates in some white-rot fungi, such as *Ceriporiopsis subvermispora*, *P. ostreatus*, and *Dichomitus squalens* (Hori et al., 2014; Alfaro et al., 2016; Fernández-Fueyo et al., 2016; Rytioja et al., 2017).

Genes/proteins involved in the transcriptional regulation of ligninolytic system have been reported in some white-rot fungi (Toyokawa et al., 2016; Álvarez et al., 2009). In *P. ostreatus*, Feldman et al. (2017) reported that overexpression of the gene *ssp1* encoding a small secreted protein elevated the expression of *vp1* in glucose-peptone (GP) medium. Single mutations in two putative *Agaricomycetes*-specific DNA-binding transcription factor genes, *wtr1* and *gat1*, a putative chromatin remodeler gene, *chd1*, and a peroxisome biogenesis gene, *pex1*, were also shown to reduce the expression levels of specific *mnp/vp* genes as well as the wood lignin-degrading abilities of *P. ostreatus* on beech wood sawdust medium (BWS) (Nakazawa et al., 2017a; 2017b; 2019). However, the mechanisms underlying ligninolytic gene regulation in *P. ostreatus* remain far from being fully elucidated.

In addition to DNA-binding transcription factors, histone modifications have been shown to be involved in the transcriptional regulation of cellulolytic genes in some filamentous fungi, such as *Trichoderma reesei* (Xin et al., 2013; Antoniêto et al., 2014; Mello-de-Sousa et al., 2016). Histone chaperones have been shown to associate with histones and be involved in the assembly and disassembly of nucleosomes in yeasts as well as humans and mammals (Avvakumov et al., 2011; Amin et al., 2012). The human histone cell cycle regulator (HIRA) complex is composed of HIRA, CABIN1, ubinuclein-1 (UBN1), and transiently anti-silencing function 1 (Asf1), which mainly bind and deposit H3.3/H4 into chromatin (Ricketts and Marmorstein, 2017). Several previous studies have identified HIRA in yeast (Blackwell et al., 2004; Greenall et al., 2006), mammals (Tagami et al., 2004; Banumathy et al., 2009), and fruit flies (Loppin et al., 2005; Bonnefoy et al., 2007). HIRA was shown to affect some histone modifications, such as H3K4triMe (H3 lysine 4 trimethylation) in human (Li and Jiao, 2017) and H3K9ac/H3K9triMe (H3 lysine 9 acetylation/trimethylation) in budding yeast (Mizuki et al., 2011); however, to the best of our knowledge, the HIRA complex in ascomycete filamentous fungi and agaricomycetes has rarely been studied.

Here, we newly isolated a mutant strain that exhibits lower lignin-degrading capacity on BWS from *P. ostreatus* wild-type strain PC9 with an aim to explore the mechanisms underlying lignin degradation by this fungus. Our results demonstrated that the *hir1* gene, encoding a putative histone chaperon involved in chromatin remodeling, was responsible for the mutant phenotype. Further examination of the effects of *hir1* mutations on gene expression, lignocellulose degradation, and histone H3 modification status was also performed.

2. Materials and methods

2.1. Strains, culture conditions, and genetic techniques of P. ostreatus

The *P. ostreatus* strains used in this study are listed in Table 1. Yeast and malt extract with glucose (YMG) medium (Rao and Niederpruem, 1969) solidified with 2% (w/v) agar in 9 and 4 cm Petri dishes was used for routine cultures. The cultures were maintained at 28 °C under continuous darkness, unless stated otherwise. Introduction of mutations by UV irradiation was performed as described by Nakazawa et al. (2016). YMG supplemented with 27 μM $MnSO_4$ and 64 μM Remazol Brilliant Blue R (RBBR) solidified with 2% (w/v) agar in 4 cm Petri dishes (YMGMnR) was used to screen mutants defective in RBBR decolorization. RBBR is a dye used to examine ligninolytic activity in *P. ostreatus* (Vyas and Molitoris, 1995; Salame et al., 2010). Crosses and production of fruiting bodies were performed as described by Inada et al. (2001) and Nakazawa et al. (2016), respectively. Genetic analysis using F_1 progeny was performed as described by Nakazawa et al. (2017a). Transformation of the *P. ostreatus* strains, 20b and *hir1*d#1 (Table 1), was performed using protoplasts prepared from mycelial cells as described by Salame et al. (2012), with slight modifications (Nakazawa et al., 2016).

Table 1
The *P. ostreatus* strains used in this study.

Strain	Genotype/description	Source
20b	*A2B1 ku80::Cbx*^{Ra}	Salame et al. (2012)
PC9	*A2B1*	Larraya et al. (1999)
PC15	*A1B2*	Larraya et al. (1999)
#64	*A64 B64*	Nakazawa et al. (2017b)
UVRM28	*A2B1 hir1-1*	This study
*hir1*d#1	*A2B1 ku80::Cbx*^{R} *hir1::hph* / a *hir1* disruptant derived from 20b	This study
*hir1*d#2	*A2B1 ku80::Cbx*^{R} *hir1::hph* / a *hir1* disruptant derived from 20b	This study
CT*hir1*	*A2B1 ku80::Cbx*^{R} *hir1::hph fcy1::hir1(bar*^{b}*)*	This study
CT*hir1-1*	*A2B1 ku80::Cbx*^{R} *hir1::hph fcy1::hir1-1 (bar*^{b}*)*	This study
*hir1*dF_1#4	*A1B2 ku80::Cbx*^{R} *hir1::hph* / F_1 progeny from a cross between *hir1*d#1 and PC15	This study
*hir1*dF_1#6	*A1B2 ku80::Cbx*^{R} *hir1::hph* / F_1 progeny from a cross between *hir1*d#1 and PC15	This study

[a] *Cbx*^{R} indicates the carboxin resistance gene (Honda et al., 2000).
[b] The bialaphos resistance gene

The composition of beech wood (*Fagus crenata*) solid sawdust medium (BWS) used to quantify wood components degraded by each *P. ostreatus* strain was as follows: 1.9 g size-fractionated sawdust (250–500 μm), 0.1 g wheat bran, and 6.0 ml water. We also used toluene/ethanol-extracted BWS for analysis of extracellular enzyme activities and gene expression; extractives present in sawdust and wheat bran were removed by treatment with toluene and ethanol (2:1 v/v) for 1 h at 80 °C (repeated four times). In this case, the toluene/ethanol-extracted BWS was not subject to size-fractionation (almost all of the particles were smaller than 2 mm). Sawdust and wheat bran were purchased from Shinkoen (Gifu, Japan) and Nisshin Seifun (Tokyo, Japan), respectively. They contained moisture because they were simply stored at 4 °C. Strains were cultured on 6 cm glass Petri dishes containing BWS under solid condition and incubated at 28 °C as stationary culture.

2.2. Whole-genome resequencing

Genomic DNA was extracted from the mutant UVRM28 strain using the cetyltrimethylammonium bromide method, as described by Zolan and Pukkila (1986) and Muraguchi et al. (2003). The resulting genomic DNA was subjected to whole-genome resequencing on the HiSeq 2500 system (Illumina, CA, USA; 2*101 pair-end sequencing). The identification of mutations introduced into the genome of UVRM28 was performed using CLC Genomics Workbench tool version 20.0 (Qiagen, Venlo, Netherland). Firstly, the obtained paired-end raw reads were quality trimmed, followed by mapping to the reference genome

sequence (*P. ostreatus* PC9; http://genome.jgi.doe.g.,ov/PleosPC9_1/PleosPC9_1.home.html). The fixed ploidy variant detection tool was used to identify mutations located in the strain UVRM28, followed by removal of mutations that are also present in the *gat1-1* mutant strain, UVRM22 (Nakazawa et al., 2019) to limit those unique to UVRM28.

2.3. Construction of the cassettes used for targeted disruption and complementary transformation

The plasmid for *hir1* disruption was constructed as previously described by Nakazawa and Honda (2015). Briefly, a genomic fragment (Scaffold_3:509017–515295 in the genome database of *P. ostreatus* strain PC9), amplified by polymerase chain reaction (PCR) using the primer pair RM38/RM41 (Table S1), was cloned into pBluescript II KS + digested with *Eco*RV. Inverse PCR was performed using the resulting plasmid as a template with the primer pair RM39/RM40. A DNA fragment containing the hygromycin-B resistance gene was also amplified using pTN24-1 (Nakazawa et al., 2019) as a template with the primer pair TN400/M13R. The resulting two DNA fragments were fused using the GeneArt Seamless Cloning and Assembly kit (Life Technologies, CA, USA) to yield a plasmid containing the *hir1*-disrupting cassette. This plasmid was then introduced into the strain 20b to obtain *hir1* gene knockouts, namely *hir1*d#1 and *hir1*d#2 (Fig. S1).

To construct the plasmid used for complementary transformation (CT), genomic fragments containing *hir1* or *hir1-1*, including approximate 500 bp upstream and downstream regions (scaffold_3:509797–514338), were amplified from the genomic DNA of wild-type 20b strain or mutant UVRM28 strain, respectively, by PCR using the primer pair HL14/HL13 (Table S1). The plasmid pFNCB (Nguyen et al., 2020) was also linearized by inverse PCR with DN15 and TN157 primer pairs, followed by fusion with *hir1* or *hir1-1* genes separately using the GeneArt Seamless Cloning and Assembly kit (Life Technologies, CA, USA), yielding two different plasmids harboring *hir1* or *hir1-1* fragment (Fig. S1C), namely pFNCB-*hir1* or pFNCB-*hir1-1*, respectively. These plasmids contain the bialaphos resistance gene (Matsunaga et al., 2017), flanked by *fcy1* sequence at the 5′- and 3′-ends for integration into targeted the *fcy1* locus of the *hir1* deletion strain by homologous recombination. The complementary strains, named CT*hir1* and CT*hir1-1*, were obtained.

2.4. RNA-sequencing (RNA-seq) analysis and quantitative reverse transcription-PCR (qRT-PCR)

Two *P. ostreatus hir1* disruptants, *hir1*d#1 and *hir1*d#2 (Table 1), were grown on 6 cm glass Petri dishes containing toluene/ethanol-extracted BWS under solid condition and incubated at 28 °C as stationary culture for 13 days. Next, total RNAs was extracted as described by Nakazawa et al. (2017a) using the NucleoSpin RNA Plant and Fungi (Takara Bio, Shiga, Japan). Paired end raw reads were quality trimmed by the CLC Genomics Workbench tool version 20.0 (CLC Bio/Qiagen). Trimmed reads were mapped to the PC9 strain genome (http://genome.jgi.doe.g.,ov/PleosPC9_1/PleosPC9_1.home.html) using the RNA-seq analysis package in CLC with the parameters of at least 80% sequence identity over at least 80% of the read lengths. Two biological replicates were obtained for each strain. The RPKM (Reads Per Kilobase of exon per Million mapped reads) value were exported from CLC workbench for the following analysis.

Total RNAs were also extracted from the three strains grown on toluene/ethanol-extracted BWS for 9, 13, 20 and 28 days, followed by qRT-PCR as described by Nakazawa et al. (2019).

2.5. Assay for extracellular enzyme activities

Each *P. ostreatus* strain was grown on toluene/ethanol-extracted BWS for 13 and 20 days. The sawdust medium covered with mycelial cells was then harvested and suspended in 0.1 M Na-lactate buffer (pH 4.5). The samples were subjected to centrifugation at 2000*g* to remove the sawdust and mycelial cells. The resulting supernatant was used to measure guaiacol (2-methoxyphenol oxidation) oxidation activity as described by Kamitsuji et al. (2004). One unit of activity for guaiacol oxidation was defined as the amount of enzyme that increased the absorbance at 465 nm by 1.0 per min. The carboxymethyl cellulase (CMCase) and xylanase activities were assayed as described by König et al. (2002) and Wu et al. (2020). One unit of xylanase/CMCase was defined as the amount of enzyme required to liberate 1 μmol of reducing sugar as xylose/glucose per minute under the assay conditions.

2.6. Quantification of Klason lignin, xylose, and α-cellulose

Each *P. ostreatus* strain was grown on BWS for 20 and 30 days, followed by solvent extraction using toluene and ethanol (2:1, v/v). The residual amount of Klason lignin (acid-insoluble) contained in each BWS solution after cultivation of the *P. ostreatus* strains was quantified as previously described by Ritter et al. (1932). The residual amount of xylose present in BWS was quantified by HPLC using the method described by Yasuno et al. (1997) and Nakazawa et al. (2017b). To quantify the amount of α-cellulose, which reflects the level of crystalline cellulose, lignin was removed from the residual BWS using the Jayme-Wise method (Green, 1963), followed by the removal of hemicellulose by alkali extraction.

2.7. Chromatin immunoprecipitation (ChIP) analysis

Each *P. ostreatus* strain was grown on toluene/ethanol-extracted BWS for 13 days as described in chapter 2.4, followed by DNA-protein fixation. Specifically, the sawdust medium containing mycelia cells was washed and suspended in 20 ml phosphate-buffer saline (PBS; pH 7.4) containing 0.5% (v/w) formaldehyde, and then the samples were rotated at 4 °C for 40 min. Next, 2 ml of 3 M glycine was added to terminate the fixation reaction. Fixed mycelial cells released from the toluene/ethanol-extracted BWS were collected by filtering with 2 layers of fine-mesh gauzes and washed with PBS again. Samples were suspended in lysis buffer as previously described (Nakazawa et al., 2008). Chromatin samples were sheared to an average size of about 300–400 bp by sonication using the Bioruptor II sonicator (Sonic Bio, Kanagawa, Japan).

Immunoprecipitation (IP) was performed using the SimpleChIP Chromatin IP Kit with Magnetic Beads (Cell Signaling Technology, MA, USA), according to the manufacturer's instructions. The following antibodies were used in this study: anti-histone H3 (ab1791; rabbit IgG; Abcam, Cambridge, UK), anti-H3K9Ac antibodies (61252; mouse IgG; Active Motif, Carlsbad, CA, USA), and anti-H3K4diMe (H3 lysine 4 dimethylation) antibodies (ab32356; rabbit IgG; Abcam, Cambridge, UK). Anti-rabbit normal IgG antibody (2729S; Cell Signaling Technology, Danvers, MA, USA) was used as the control. The resulting purified DNA samples were subjected to quantitative PCR (qPCR) analysis. The number of chromatin-derived segments precipitated with each antibody was examined using the primer listed in Table S4. The SimpleChIP Universal qPCR Master Mix kit (Cell Signaling Technology, MA, USA) was used for PCR. The real-time PCR reaction was carried out in a total volume of 10 μl containing 0.5 μM primers and 1X SimpleChIP qPCR master mix (Cell Signaling Technology, MA, USA), 0.2 μM primers and 1X KOD SYBR qPCR master mix (TOYOBO, Osaka, Japan), or 0.2 μM primers and 1X GoTaq qPCR master mix (Promega, WI, USA). The PCR conditions were as follows: for SimpleChIP, one cycle at 95 °C (3 min) for initial denaturation, 40 cycles at 95 °C (15 sec) and 60 °C (60 sec), followed by the melting curve generation from 60 to 95 °C; for KOD, one cycle at 98 °C (2 min) for initial denaturation, 40 cycles at 98 °C (10 sec), 60 °C (10 sec), 68 °C (30 sec), followed by the melting curve generation from 60 to 95 °C; for GoTaq, one cycle at 95 °C (2 min) for initial denaturation, 40 cycles at 95 °C (15 sec) and 60 °C (60 sec), followed by the melting curve generation from 60 to 95 °C. The efficiency of each

primer set was also examined using the same procedure (Table S4). The amplification efficiency (Table S4) of each primer pair was determined by analyzing a serially diluted target; the DNA samples were diluted in 10-fold increments (total of four samples with concentrations of 1 to 10^{-3}), and the threshold cycle (Ct) value yielded by each primer was evaluated. The IP efficiency was calculated by relative quantification of the immunoprecipitated sample and 2% input using the Thermal Cycler Dice Real Time System *Lite* (Takara, Shiga, Japan).

3. Results

3.1. Isolation and genetic analysis of a *P. ostreatus* mutant UVRM28

We newly isolated a *P. ostreatus* mutant defective in decolorization of RBBR present in the YMGMnR agar medium, namely UVRM28, after UV mutagenesis of wild-type strain PC9 (Table 1). RBBR is frequently used to examine the ligninolytic activity of *P. ostreatus* (Vyas and Molitoris, 1995; Salame et al., 2010). To confirm whether the wood lignin-degrading ability of this strain was reduced, PC9 and UVRM28 strains were grown on BWS for 28 days. Results showed that about 30% of Klason lignin was degraded in plates growing the PC9 strain, whereas almost no loss of Klason lignin was observed after growing the UVRM28 strain (Fig. S2). Thus, these findings suggest that the ability of the mutant strain to degrade wood lignin was significantly reduced when grown on BWS.

To identify a gene mutation(s) responsible for the mutant phenotypes of the strain UVRM28, genetic analyses were performed. UVRM28 was mated with a wild-type monokaryon PC15. The resulting dikaryon decolorized RBBR present in the YMGMnR agar medium, similar to the monokaryon strain PC9 (data not shown). This result suggests that the mutant phenotype of UVRM28 is recessive. We then isolated F_1 progeny from a cross between UVRM28 and PC15, followed by linkage analysis using eight F_1 progeny (four strains that decolorized RBBR and the other four defective in decolorization) to identify a genomic region(s) containing or located close to a responsible gene. Genomic PCR was performed using primer pair 3-2f/3-2r, which amplifies the 633-bp fragment (corresponding to the region around Scaffold_3: 600000 in the genome of PC9) from the genomic DNA derived from PC15, but not from PC9 due to the difference in genome sequence between the two *P. ostreatus* strains. Similarly, 2-5f/2-5r (2-5_PC9) and 8-1f/8-1r (8-1_PC9) amplify 785-bp and 760-bp genomic fragments (corresponding to the region around Scaffold_2: 2100000 and Scaffold_8:100000 in the genome of PC9) from PC9, but not from PC15, respectively. We used these PCR fragments as a genetic marker (3-2_PC15). In the case of the marker 3-2_PC15, the fragments from the genome of the four F_1 strains that decolored RBBR were amplified, but those from the four strains that did not, were not amplified (Fig. 1A; recombination value, 0; 0/8), whereas recombination values for 2-5_PC9 and 8-1_PC9 were 50 (4/8) and 37.5 (3/8), respectively (data not shown). Furthermore, linkage analysis was also performed using 16 F_1 progeny isolated from a cross between PC9 and PC15, all of which decolorized RBBR normally, as a control. The marker 3-2_PC15 was not linked among them (Fig. 1B; recombination value, 56; 9/16) These results suggest that a gene mutation (s) responsible for the mutant phenotypes of UVRM28 may be located in the genomic region close to the marker 3-2_PC15.

3.2. Identification of the hir1-1 mutation

To identify a gene mutation(s) in the UVRM28 genome close to the genetic marker 3-2_PC15, we performed whole-genome resequencing of this strain (Table S2). Total 82 non-synonymous variants were identified in the genome of strain UVRM28 (Table S5) with the greatest number of single nucleotide variants and a small amount of indels. Based on this result and the linkage analysis, we identified a nonsense mutation in the gene located in Scaffold_3: 510478–513842 (Protein ID 115161; Fig. 2, S1C, and S3). This mutation was not found not only in UVRM22 but also

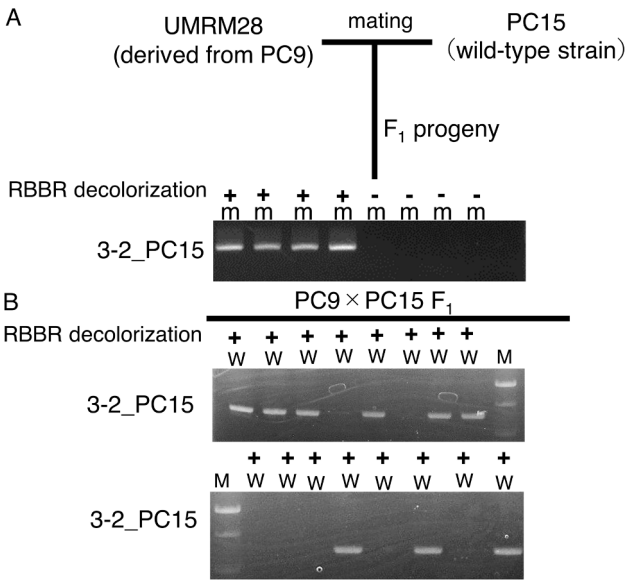

Fig. 1. Identification of the genetic marker 3-2_PC15 closely linked to the mutant phenotype. A, the marker 3-2_PC15 was amplified in F_1 progeny inheriting the genomic region around the marker PC15. "+" refers to the F_1 progenies that decolorized RBBR, "–" refers to the F_1 progenies that failed to decolorize RBBR. B, amplifying marker 3-2_PC15 in 16 F_1 progenies isolated from a cross between PC9 and PC15.

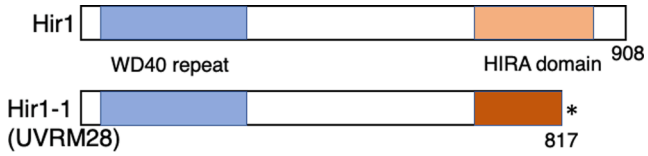

Fig. 2. The putative Hir1 structure based on BLAST search. The effect of *hir1-1* mutations on protein function is indicated.

in the other mutant strains the genomes of which were sequenced such as UVRM24 (data not shown) and UVRM25 (Fig. S3). These results suggest that the aforementioned gene mutation may be responsible for the mutant phenotypes of UVRM28.

Protein ID 115161 encoded by this gene is highly conserved among fungi, including agaricomycete species, such as *Coprinopsis cinerea* Hir1 homolog (60.02% identity; NCBI reference sequence, XP_001839016) and *Trametes versicolor* Hir1 homolog (62.70% identity; NCBI reference sequence, XP_008041329), and ascomycete species, such as *Schizosaccharomyces pombe* Hip1 (44% identity; NCBI reference sequence, P87314) (Blackwell et al., 2004), *Saccharomyces cerevisiae* Hir1 (39.57% identity; NCBI reference sequence, CAA84827) (Sherwood et al., 1993; DeSilva et al., 1998), and *Neurospora crassa* Hir1 (39% identity; NCBI reference sequence, XP_957650). The Hir1 protein in *P. ostreatus* was found to be more closely related to that in agaricomycete Hir1 homolog types and yeast Hir1 and Hir2 types (Fig. 3). Based on this homology search, we designated the *P. ostreatus* gene corresponding to Protein ID 115161 as *hir1*. The protein encoded by this gene has two motifs, the N-terminal WD40 repeat and a HIRA C-terminal domain. The WD40 repeat is a short motif structure containing approximately 40 amino acids and often terminates in a tryptophan-aspartic acid (W-D) dipeptide. These repeats specifically fold together to form a tubular structure. Both of the above two motifs are involved in histone chaperone complex formation. The former interacts with UBN1, and the latter with CABIN1, both of which are reported to be important for maintaining the structural integrity of the human HIRA complex (Banumathy et al., 2009; Rai et al., 2011). We found that the mutation was located at the Q817 position (Fig. 2), which resulted in a stop codon to interrupt the translation of the

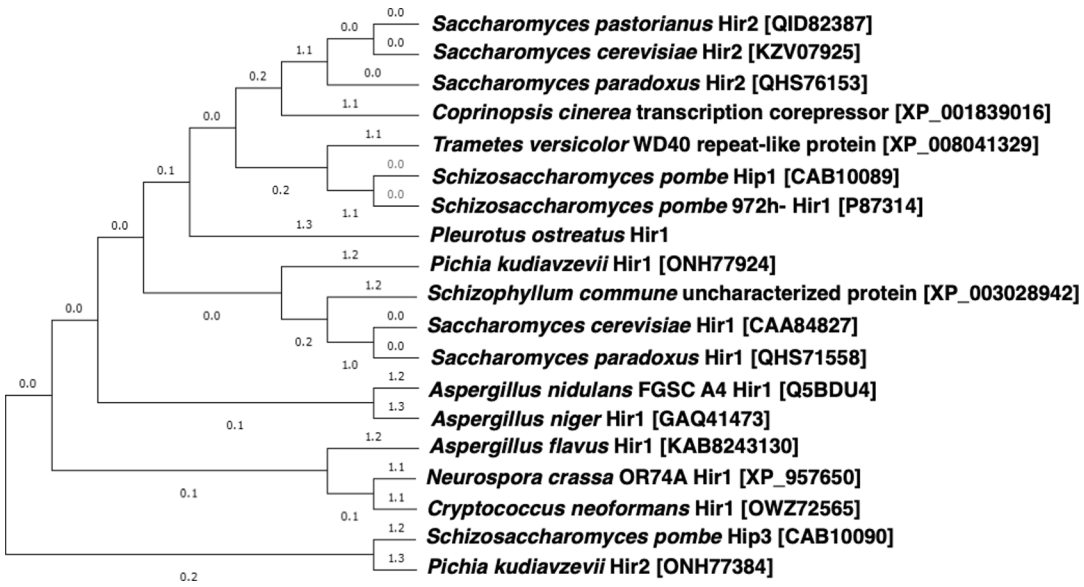

Fig. 3. Neighbor-joining phylogenetic tree of the homologs of Hir1 proteins generated with MEGA 10.1.8 software based on the BLAST database from NCBI. The accession numbers for each sequence of each protein in the NCBI are presented in brackets.

HIRA C-terminal domain, suggesting that the interaction between the HIRA C-terminal domain and CABIN1 cannot function well if the mechanisms/functions of histone chaperones are conserved between Human and Basidiomycetes. Based on these results, we designated the possible gene mutation responsible for the mutant phenotypes of UVRM28 as *hir1-1*.

3.3. Effects of hir1 mutations on lignin-degrading ability in BWS

Considering that the *hir1-1* mutation may be responsible for the mutant phenotypes of UVRM28, two *hir1* disruptants, *hir1*d#1 and *hir1*d#2, were generated from the parental strain 20b (Fig. S1) to examine their phenotypes. To analyze the effects of *hir1* disruption on hyphal growth rate, these three strains were grown on a YMG agar plate for 6 days. Results showed that the growth rates of the *hir1* disruptants were almost similar to those of their parental strain, 20b (Fig. S4). Next, we compared the extracellular manganese-dependent peroxidase (MnP) activity and lignin-degrading abilities of the *hir1* disruptants and 20b strain to examine the effects of *hir1* disruption on the ligninolytic system. Extracellular MnP activities were determined after growing each strain on toluene/ethanol-extracted BWS for 13, 20, and 30 days. As shown in Fig. 4, MnP activity was much lower in the *hir1* disruptants than that in the 20b strain at any given time point, indicating that *hir1*d#1 and *hir1*d#2 lost their extracellular MnP activities. Two *hir1* disruptants and 20b were also cultured on BWS for 20 and 30 days to compare their abilities to degrade wood lignin. As shown in Fig. 5, the decrease in the amount of Klason lignin in the medium after growing the *hir1* disruptants was much lower than that after growing the 20b strain, suggesting that disruption of *hir1* reduced lignin-degrading ability on BWS.

To testify whether the mutation *hir1-1* alone was responsible for the mutant phenotypes of UVRM28, a plasmid containing *hir1* gene fragments (pFNCB-*hir1* and pFNCB-*hir1-1*) cloned from 20b and UVRM28 was separately transformed to *hir1*d#1 disruptants. Bialaphos-resistant transformants were obtained, following which they were transferred onto YMG medium containing 0.1% 5-FC to select *fcy1*-deficient strains in which *hir1* or *hir1-1* was inserted into the *fcy1* locus. Finally, the screened transformants were subjected to genomic PCR using the primers TN101/TN102, TN101/TN762, and DN15/TN102 (Table S1) to confirm the insertion (data not shown). Two strains, CT*hir1* and CT*hir1-1*, were obtained (Table 1). To examine whether the complementation of *hir1*, but not that of *hir1-1* mutation, rescues one of the mutant

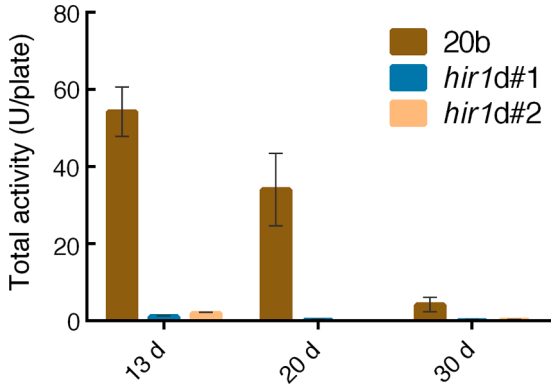

Fig. 4. Examination of MnP activities of strain 20b and *hir1* disruptants when grown on BWS for 13, 20, and 30 days. The bars represent standard deviation (n = 3). One unit of activity for guaiacol oxidation was defined as the amount of enzyme that increased the absorbance at 465 nm by 1.0 per min.

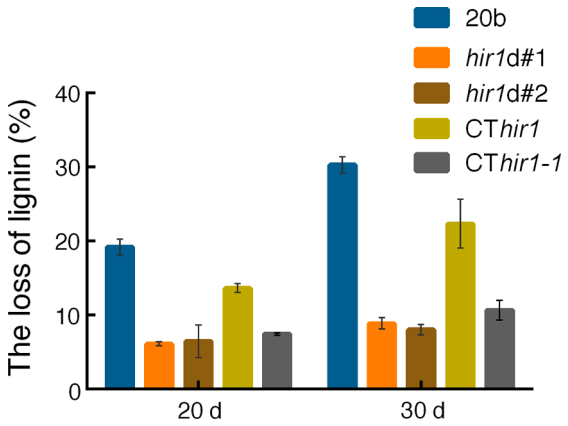

Fig. 5. Degradation of Klason lignin by *hir1* disruptants, 20b strain, and the complementary transformants CT*hir1* and CT*hir1-1*. All strains were grown on BWS for 20 and 30 days. The bars represent standard deviation (n = 3). The decrease in the amount of Klason lignin per plate was compared with that in the No-fungus control plate (onto which *P. ostreatus* had not been inoculated).

phenotypes (defects in wood lignin degradation) of *hir1*d#1, CT*hir1* and CT*hir1-1* strains were cultured on BWS for 20 and 30 days. The decrease in the amount of Klason lignin by CT*hir1* strain was larger than that by *hir1*d#1, while as for CT*hir1*-1 strain, the decrease amount was similar to that by *hir1*d#1 (Fig. 5). In this study, complementary transformation of UVRM28 with *hir1*$^{+}$ was not performed because the growth rate of UVRM28 became lower after long-term storage. These results suggest that *hir1* may be the only gene responsible for UVRM28 phenotypes.

3.4. Transcriptional alterations of putative ligninolytic genes in hir1 disruptants

To examine the effects of *hir1* disruption on transcriptional gene expression, we performed RNA-seq on 20b strain and *hir1* disruptants (Table S3). The RPKM values for *mnp/vp* genes are listed in Table 2. It was previously shown that the accumulation of *vp2* transcript was most abundant in strain 20b grown on toluene/ethanol-extracted BWS for 13 days, but was significantly reduced in all mutant strains exhibiting reduced lignin-degrading abilities in BWS, which we obtained/characterized in our previous studies (Nakazawa et al., 2019; Wu et al., 2020). Here, the RPKM value of *vp2* was much lower in *hir1* disruptants than that in 20b (about one-thousandth), indicating that *vp2* transcript accumulation was reduced in *hir1* disruptants as well as the other ligninolysis-deficient mutant strains. In contrast to *vp2*, the RPKM value of *vp1*, which was the lowest among *vp/mnp* genes in strain 20b grown on BWS for 13 days, was much higher in *hir1* disruptants (about 300–400 fold at RPKM value). Moreover, the RPKM values of *mnp3* and *mnp6* were also higher in *hir1* disruptants. These results indicate that the accumulation of *vp2* transcript was decreased, while that of *vp1*, *mnp3*, and *mnp6* was elevated, in *hir1* disruptants. In addition, the RPKM values of three genes encoding putative glyoxal oxidases (GLOX; AA5 family, Protein IDs 77373, 96655, and 62347) were shown to be very high in strain 20b, but much lower in *hir1* disruptants (1/30–1/100 in RPKM values), which is consistent with the results of the other four ligninolysis-deficient strains previously analyzed.

Table 2
RPKM values of ligninolytic genes including *vps/mnps* and *glox* in *hir1* disruptants and 20b strain.

CAZy	Gene or protein ID[a]	RPKM			FC[b]	
		20b[c]	*hir1*d#1[d]	*hir1*d#2[d]	*hir1*d#1	*hir1*d#2
AA2	*vp1*	2.11	882.57	636.06	418.32	301.48
	vp2	3601.27	41.10	21.31	0.01	0.01
	vp3	916.18	265.58	196.58	0.29	0.21
	mnp1	11.39	14.63	13.21	1.28	1.16
	mnp2	171.80	292.84	274.36	1.70	1.60
	mnp3	248.35	711.91	685.23	2.87	2.76
	mnp4	17.60	32.05	29.17	1.82	1.66
	mnp5	9.96	1.75	1.35	0.18	0.14
	mnp6	125.79	578.26	503.14	4.60	4.00
AA5	121363	0.20	0.37	0.24	1.83	1.19
	91068	2.47	3.14	4.40	1.27	1.78
	84350	22.76	27.15	30.03	1.19	1.32
	88952	31.40	35.41	41.87	1.13	1.33
	67424	77.40	72.95	83.51	0.94	1.08
	94009	4.50	3.26	4.73	0.72	1.05
	62166	264.11	174.52	272.93	0.66	1.03
	98389	24.55	14.79	19.00	0.60	0.77
	134564	765.38	452.28	756.51	0.59	0.98
	101121	41.57	14.79	19.00	0.60	0.77
	99670	15.66	4.91	4.40	0.31	0.28
	89214	57.53	9.71	11.82	0.17	0.21
	77373	190.79	28.83	31.08	0.15	0.16
	96655	463.86	22.95	21.93	0.05	0.05
	62347	425.54	17.46	18.10	0.04	0.04

[a] A genomic fragment containing the genes that corresponds to each Protein ID were from the genome database of strain PC9 (JGI *Pleurotus ostreatus* PC9 v1.0, https://genome.jgi.doe.gov/PleosPC9_1/PleosPC9_1.home.html).
[b] FC, fold change. Ratios were calculated by comparing the RPKM value of *hir1* disruptants and that of the parental control strain 20b.
[c] RPKM value used in this table was the average value of duplicated data from 20b.
[d] RPKM value used in this table was the average value of two data from *hir1*d#1 and *hir1*d#2, respectively.

3.5. Upregulation of putative cellulolytic and xylanolytic genes in hir1 disruptants

Previously, it was shown that cellulolytic and xylanolytic genes were activated at the transcription level in *pex1* and *gat1* single-gene disruptants from 20b and the *chd1-1* mutant strain (UVJ3-3) from PC9 (Wu et al., 2020). The RPKM values for the major cellulolytic and xylanolytic genes, GH6, GH7, GH10, GH11, and AA9, are listed in Table 3 and Table 4. The RPKM values of putative cellulolytic genes, which encode copper-dependent lytic polysaccharide monooxygenases belonging to the AA9 family, putative endo-β-1,4 glucanases belonging to GH6 (Protein ID 43698), and GH7 (Protein IDs 83320 and 83849) significantly increased in the *hir1* disruptants, which is very similar to the case of the three mutant strains (Δ*gat1*, Δ*pex1*, and *chd1-1*; Wu et al., 2020). However, analysis of the transcript levels of genes encoding putative xylanases showed that four genes (Protein IDs 81650, 110996, 125911, and 89740) were upregulated and one gene (Protein ID 96691) was significantly downregulated, thus indicating that the expression of xylanolytic genes was altered rather than simply upregulated.

3.6. Time-course expression patterns of some of the lignocellulolytic enzyme-encoding genes

In this study, RNA-seq was performed on 20b, *hir1*d#1 and *hir1*d#2 at 13-day culture period only. Considering that different growth periods could result in gene expression bias in some wood-decaying fungi (Hori et al., 2014; Alfaro et al., 2016; Fernández-Fueyo et al., 2016; Rytioja

Table 3
RPKM values of cellulolytic genes encoding endo-β-1,4 glucanases belonging to GH6 and GH7 in *hir1* disruptants and 20b strain.

CAZy	Protein ID[a]	RPKM			FC[b]	
		20b[c]	*hir1*d#1[d]	*hir1*d#2[d]	*hir1*d#1	*hir1*d#2
GH6	43698	1.18	110.77	109.93	93.95	93.23
	130231	1.78	26.30	13.19	14.75	7.40
	45206	194.51	1241.56	934.31	6.38	4.80
GH7	83320	1.38	372.63	413.46	270.89	300.57
	83849	6.71	441.82	350.61	65.82	52.23
	49686	40.31	312.55	212.62	7.75	5.28
	90281	2.49	6.18	4.89	2.48	1.96
	114771	482.61	1264.11	951.68	2.62	1.97
	100231	4.40	8.14	7.60	1.85	1.73
	49445	229.29	508.89	276.27	2.22	1.20
	107842	6.58	12.24	8.27	1.86	1.26
	129772	2.45	2.81	3.30	1.15	1.35
	90565	6.08	6.75	6.85	1.11	1.13
	94368	3.05	2.52	2.37	0.83	0.78
	129783	10.79	8.75	8.46	0.81	0.78
	83987	28.45	23.64	21.22	0.83	0.75
	100398	1.82	1.20	1.02	0.66	0.56
	47406	2.13	1.16	0.76	0.55	0.36
	47295	31.95	5.39	3.54	0.17	0.11

[a] A genomic fragment containing the genes that corresponds to each Protein ID were from the genome database of strain PC9 (JGI *Pleurotus ostreatus* PC9 v1.0, https://genome.jgi.doe.gov/PleosPC9_1/PleosPC9_1.home.html).
[b] FC, fold change. Ratios were calculated by comparing the RPKM value of *hir1* disruptants and that of the parental control strain 20b.
[c] RPKM value used in this table was the average value of duplicated data from 20b.
[d] RPKM value used in this table was the average value of two data from *hir1*d#1 and *hir1*d#2, respectively.

Table 4
RPKM values of genes encoding LPMOs belonging to AA9 and xylanases belonging to GH10 and GH11 in *hir1* disruptants and 20b strain.

CAZy	Protein ID[a]	RPKM			FC[b]	
		20b[c]	*hir1*d#1[d]	*hir1*d#2[d]	*hir1*d#1	*hir1*d#2
AA9	44265	4.41	152.29	115.13	34.51	26.09
	97339	9.92	519.44	446.76	52.34	45.02
	96461	7.54	326.64	266.94	43.34	35.42
	59310	4.19	46.25	87.12	11.04	20.79
	46220	101.05	1036.63	1019.68	10.26	10.09
	100006	135.39	1028.25	981.79	7.59	7.25
	122311	188.13	1275.77	1152.04	6.78	6.12
	21397	3.32	46.44	37.18	13.99	11.20
	94230	4.43	62.01	44.08	13.98	9.94
	56431	99.91	459.70	337.40	4.60	3.38
	100072	769.77	1417.13	1559.89	1.84	2.03
	45362	14.24	22.10	22.03	1.55	1.55
	125666	2.41	4.04	3.94	1.68	1.64
	134258	13.37	17.88	22.95	1.34	1.72
	94095	5.99	13.11	8.21	2.19	1.37
	130437	1.09	2.46	2.21	2.26	2.03
	117057	398.05	397.03	446.10	1.00	1.12
	46385	9.63	10.93	10.49	1.14	1.09
	134259	24.42	16.39	15.78	0.67	0.65
	20839	96.10	38.04	42.03	0.40	0.44
	21077	13.76	1.87	1.67	0.14	0.12
GH10 and GH11	110996	7.21	328.42	209.86	45.56	29.11
	125911	10.62	204.37	125.74	19.25	11.84
	89740	426.61	1544.65	1432.81	3.62	3.36
	81650	424.87	899.64	706.88	2.12	1.66
	96691	199.16	19.40	15.52	0.10	0.08

[a] A genomic fragment containing the genes that corresponds to each Protein ID were from the genome database of strain PC9 (JGI *Pleurotus ostreatus* PC9 v1.0, https://genome.jgi.doe.gov/PleosPC9_1/PleosPC9_1.home.html).
[b] FC, fold change. Ratios were calculated by comparing the RPKM value of *hir1* disruptants and that of the parental control strain 20b.
[c] RPKM value used in this table was the average value of duplicated data from 20b.
[d] RPKM value used in this table was the average value of two data from *hir1*d#1 and *hir1*d#2, respectively.

et al., 2017; Zhang et al., 2019), qRT-PCR was also performed on the three *P. ostreatus* strains at 9-, 20- and 28-day culture periods to examine time-course expression patterns of some of the differentially expressed lignocellulolytic enzyme-encoding genes. As shown in Fig. S6, the expression levels of the upregulated (downregulated) genes at the 13-day culture period were also overall higher (lower) in the *hir1* disruptants at almost of the all culture periods; however, various expression patterns were observed. For examples, the expression level of one gene (Protein ID 97339) was higher in the disruptants at all the four culture periods, and reached the highest at 28 days. Those of other three genes (Protein IDs 83320, 43698 and *vp1*) reached the highest at 13-day culture period in the disruptants. Most notably, the four ligninolytic enzyme-encoding genes highly expressed in 20b grown on BWS for 13 days but not in the disruptants (*vp2*, *vp3*, 62347 and 96655) were shown to be significantly downregulated at all the culture periods. This result suggests that major ligninolytic system is constitutively inactive in the *hir1* disruptants.

3.7. Hir1 is not essential for fruiting development in P. ostreatus

Considering that Hir1 is a putative histone chaperone, *hir1* disruption may cause not only defects in wood lignin degradation but pleiotropic effects; therefore, we also examined the effects of *hir1* disruption on fruiting development as described by Nakazawa et al. (2017b). Two F_1 strains from a cross between *hir1*d#1 and PC15 with the *A1B2* and resistance to hygromycin B were used as tester strains, which were designated as *hir1*dF_1#4 and *hir1*dF_1#6 (Table 1). In this experiment, hygromycin-resistant strains were considered as *hir1* disruptants and sensitive as *hir1*$^+$. Strain *hir1*dF_1#4 was mated with four F_1 progeny from a cross between *hir1*d#1 and #64 (three were hygromycin-B sensitive and one resistant). The *hir1*dF_1#6 was also mated with one hygromycin-resistant F_1 progeny from a cross between *hir1*d#1 and #64, and with five F_1 progeny from a cross between *hir1*d#2 and #64 (two were hygromycin-B sensitive and three resistant). All of the resulting dikaryon strains formed fruiting bodies. This result suggests that *hir1* is not essential for fruiting in *P. ostreatus*.

3.8. Effects of hir1 disruption on extracellular CMCase and xylanase activities

Considering that many putative cellulolytic and xylanolytic genes were upregulated in *hir1* disruptants, extracellular CMCase and xylanase activities were examined in *hir1*d#1 and 20b grown on BWS for 13, 20, and 30 days to determine whether the upregulation of these enzyme-encoding genes affected extracellular enzyme activities (Fig. 6). Results showed that both of the extracellular CMCase and xylanase activities were higher in *hir1*d#1 than those in 20b strain when grown on BWS for 13 and 20 days, but not for 30 days.

3.9. Effects of hir1 disruption on the ability to degrade xylan and cellulose in BWS

We compared the xylan an α-cellulose loss after culturing these strains on BWS for 20 and 30 days as a mean of determining the effects of *hir1* disruption on cellulolytic and xylanolytic activities. As shown in Fig. 7, a significant difference was not observed, although substrates cultured with 20b exhibited a slightly higher decrease in both cellulose and xylan amounts than those cultured with *hir1* disruptants for 30 days. These results suggest that *hir1* disruption significantly reduces the

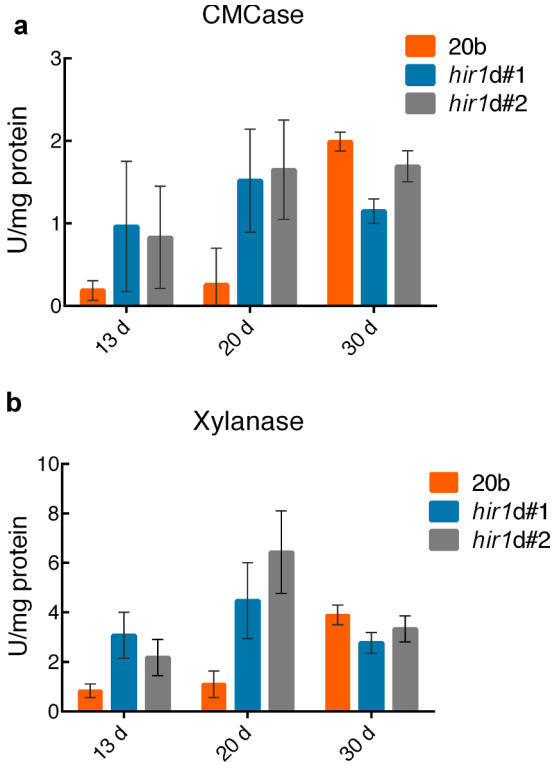

Fig. 6. The specific extracellular CMCase and xylanase activities of the indicated strains grown on BWS for 13, 20, and 30 days. One unit of xylanase/CMCase (U) is defined as the amount of enzyme required to liberate 1 μmol of reducing sugar as xylose/glucose per minute under the assay conditions. Error bars represent the standard deviations of three bioreplicates.

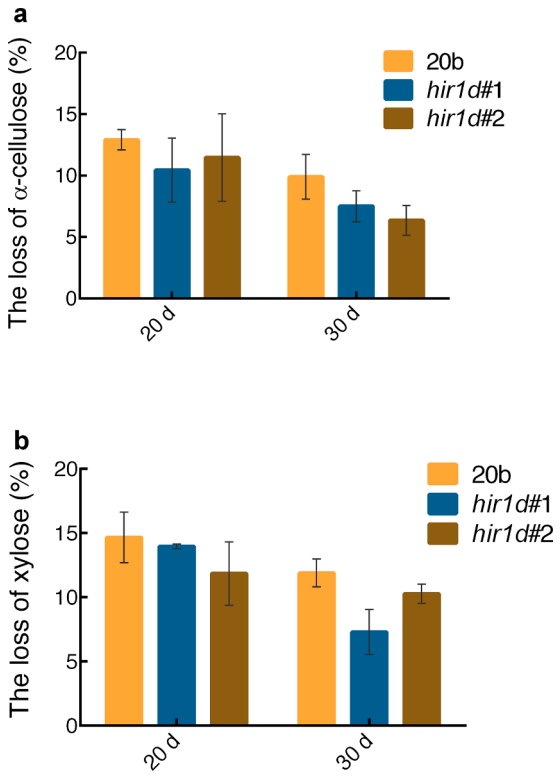

Fig. 7. Degradation of α-cellulose and a polysaccharide composed of xylose by *hir1* disruptants and 20b strain. All strains were grown on BWS for 20 and 30 days. The decrease in the amount of xylose per plate was compared with that in the No-fungus control plate (onto which *P. ostreatus* had not been inoculated). Cellulose loss was determined by measuring the decrease in the amount of α-cellulose in the substrate relative to the No-fungus control plate. Xylan loss was determined by examining the amount of xylose after the sulfuric acid hydrolysis of the substrate relative to the No-fungus control plate. The bars represent standard deviation (n = 3).

capacity of *P. ostreatus* to degrade lignin, but did not affect xylan and cellulose degradation, in BWS.

3.10. Effects of hir1 disruption on H3K4diMe and H3K9Ac levels in the 5′-upstream regions of some lignocellulolytic genes

Considering that the HIRA complex was involved in some histone modifications in fission yeast (Mizuki et al., 2011), we performed the chromatin immunoprecipitation assay to explore the relationship between histone modifications and transcriptional changes in lignocellulolytic genes. Here, we examined H3K4diMe and H3K9Ac levels because these modifications have been most frequently analyzed and shown to be involved in transcriptional gene regulation in some ascomycete filamentous fungi, such as *Aspergillus nidulans* and *Magnaporthe oryzae* using commercially available antibodies (Bok et al., 2009; Pham et al., 2015). The IP efficiency of normal IgG was very low (data not shown) in all genes listed in Fig. 8e. Results (Fig. 8a) showed that the immunoprecipitation efficiencies (H3K4diMe) in the 5′-upstream regions of one ligninolytic (*vp1*) and two cellulolytic (Protein IDs 43698 and 44265) genes upregulated in the *hir1* disruptants were higher in the *hir1* disruptants than those in strain 20b. The IP efficiencies (H3K9Ac) of *vp1* and some of the upregulated cellulolytic genes (Protein IDs 81650 and 43698; Fig. 8c) were also higher in *hir1* disruptants than those in strain 20b. Furthermore, all IP efficiencies (both H3K4diMe and H3K9Ac) of the downregulated *vp* and *glox* genes (*vp2*, *vp3*, 62347, and 96655; Fig. 8b, 8d) did not show much difference between 20b strain and *hir1* disruptants in this study except for the case of H3K4diMe of 96655. The 5′-upstream regions of one downregulated xylanase gene (Protein ID 96691) also showed lower H3K4diMe IP efficiency. These results suggest that H3K4diMe and/or H3K9Ac levels in the 5′-upstream regions of several lignocellulolytic genes are altered in *P. ostreatus hir1*disruptants.

4. Discussion

In this study, a mutation in the *hir1* gene encoding a putative component of histone chaperone protein (homolog to human HIRA) was shown to decrease the lignin-degrading ability of *P. ostreatus* in BWS. HIRA is a histone chaperone highly conserved throughout the evolution from yeast to humans. Several HIRA homologs have been identified, such as Hip1 in *S. pombe* (Blackwell et al., 2004), and Hir1 and Hir2 as transcriptional regulators of histone genes in *S. cerevisiae* (Sherwood

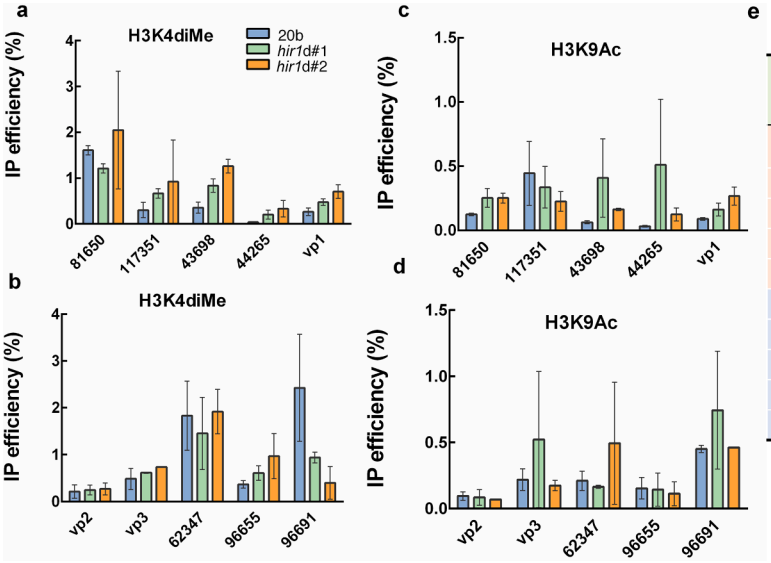

Gene or Protein ID	CAZy	Δ*hir1*
81650	GH10	activation
117351	CE1	activation
43698	GH7	activation
44265	AA9	activation
vp1	AA2	activation
vp2	AA2	inactivation
vp3	AA2	Inactivation
62347	AA5	inactivation
96655	AA5	Inactivation
96691	GH10	inactivation

Fig. 8. Examination of H3K4diMe and H3K9Ac levels in the 5′-upstream regions of each gene of *hir1* disruptants by ChIP analysis. IP efficiency was calculated by relative quantification of the immunoprecipitated sample and 2% input. Primer pairs (Table S4) amplifying the 5′-upstream regions (around 500 bp upstream of the start codon) of each gene were used for qPCR. The bars represent standard deviation (n = 2).

et al., 1993). This study suggested that Hir1 might play a role in transcriptional regulation of some lignocellulolytic genes in *P. ostreatus* by affecting histone modification patterns.

Although *hir1-1* is considered to be responsible for the mutant strain UVRM28, the lignin-degrading abilities of mutant strain UVRM28 (*hir1-1*) and disruptant strains (Δ*hir1*) may not be completely identical as about 7% lignin could be degraded by *hir1* disruptants and CT*hir1-1*, while almost no lignin was degraded by UVRM28 strain. Furthermore, unlike our previous studies (Nakazawa et al., 2016; 2017a; 2017b), we performed neither extensive linkage analysis using many other primer pairs/genetic markers nor complementation test of UVRM28. In light of these facts, we cannot exclude the possibility of other mutations present in the UVRM28 strain, which may influence its lignin-degrading ability.

Our results showed that *hir1* disruptants lost their extracellular MnP activity when grown on BWS for either 13 or 20 days, but slightly retained their lignin-degrading capacity in BWS. Considering that there are numerous lignin-modifying enzymes secreted by *P. ostreatus*, such as laccases, VPs, and MnPs, which showed different expression patterns in *hir1* disruptants; in addition, enzymes apart from the above-mentioned ones could also play a role in lignin decomposition/degradation, thus total inactivation of Mnp activity may not always result in the complete loss of lignin-degrading capacity. Unlike the four mutations we identified in our previous study (Wu et al., 2020), *hir1* disruptants displayed alterations in the expression of ligninolytic genes rather than drastic inactivation. On comparing the sum of RPKM values of all *vps/mnps*, results showed that *hir1* disruptants retained 50% of the transcripts as compared with that in the parental strain 20b (Fig. S5). In addition, *hir1* disruptants showed higher expression of genes encoding laccases than the parental strain 20b (Fig. S5). This could be recognized as a functional redundancy within the ligninolytic gene families of *P. ostreatus*, as this characteristic feature has also been previously suggested by Salame et al. (2013).

Here, our results showed that many cellulolytic genes encoding enzymes from GH6, GH7, and AA9 were remarkably upregulated, and xylanolytic genes encoding enzymes classified into GH10 and GH11 were also upregulated, except one gene (Protein ID 96691), which was downregulated in *hir1* disruptants in BWS. This is in line with our previous observation in most of the *P. ostreatus* mutants with defects in the ligninolytic system in BWS (Wu et al., 2020). We observed similar transcriptional alterations with regard to the upregulation of cellulolytic and xylanolytic genes in all five ligninolytic deficient mutants (*chd1-1*, Δ*pex1*, Δ*gat1*, Δ*wtr1*, and Δ*hir1*), which reflected that some identical regulation mechanisms might be triggered in *P. ostreatus* mutant strains. It is still unclear by which mechanisms these regulation switches being triggered; this should be clarified in future studies.

Altering histone chaperones could result in histone modifications and therefore affect the transcription of target genes. In this study, higher and lower H3K4diMe and/or H3K9Ac levels in some of the up- and down-regulated lignocellulolytic genes were observed in *hir1* disruptants, respectively, suggesting association of these histone modifications with the transcriptional regulation (especially upregulation) of the lignocellulolytic genes in *P. ostreatus*. In our previous study, mutations in the gene *chd1*, which encodes a putative chromatin remodeling factor, were shown to cause defects in the ligninolytic system in BWS (Nakazawa et al., 2017a). Transcriptional analysis showed that many cellulolytic genes were also upregulated in the *chd1-1* mutant strain grown on BWS (Wu et al., 2020). Chd1 is a member of the chromodomain helicase DNA-binding (CHD) family, which is highly conserved in eukaryotes (Marfella and Imbalzano, 2007). It was reported that the loss of *S. cerevisiae* Chd1 globally altered histone modification patterns (H3K4me3 and H3K36me3) with respect to active transcription (Radman-Livaja et al., 2012). This suggests that the activation of cellulolytic genes could be attributed to histone modifications. In this study, we examined two histone modification patterns (H3K4diMe and H3K9Ac). However, other histone modification patterns which might be affected by *hir1* modifications cannot be excluded as Dutta et al. (2010) reported that the protein HIRA could mediate the incorporation of Lys-56-acetylated H3.3 molecules at the *Vegfr1* (vascular endothelial growth factor receptor 1) chromatin domain in mammals. Therefore, the H3K56Ac level may also be altered in *P. ostreatus hir1* disruptants, which should be explored in future studies. Furthermore, effects of *hir1* disruption on the global histone modification patterns (not only in 5′-upstream regions of some genes) should be analyzed by ChIP-seq coupled with RNA-seq to reveal other function(s)/role(s) of Hir1 (and HIRA complex) in transcriptional regulation in *P. ostreatus*.

In conclusion, we identified a mutation in *hir1*, which encodes a putative component of histone chaperone, as a modifier to mediate ligninolytic, cellulolytic, and xylanolytic system directly or indirectly in the Basidiomycete *P. ostreatus*. Our findings provide a clue with respect to the correlations between alterations in the expression of some lignocellulolytic genes and histone modification of H3K4diMe and/or H3K9Ac. However, the possibility that other histone modifications may have major effects on transcriptional gene expression cannot be excluded. This should be investigated in future studies to advance our understanding of regulatory mechanisms governing lignocellulose degradation.

CRediT authorship contribution statement

T.N. conceived and designed the study. T.N., H.L.W., R.M., Shivani carried out the experiment. T.N. and H.L.W. drafted the manuscript. T. N. and H.L.W. performed the analyses, M.S. and Y.H.provided editorial suggestions and revisions.

Acknowledgments

This work was supported in part by the Institute of Fermentation, Osaka [to T.N (no grant number)], JSPS KAKENHI (to T.N; 16K18729 and 19H03017), and the China Scholarship Council (to H.W).

Appendix A. Supplementary material

Supplementary data to this article can be found online at https://doi.org/10.1016/j.fgb.2020.103507.

References

Alfaro, M., Castanera, R., Lavín, J.L., Grigoriev, I.V., Oguiza, J.A., Ramírez, L., Pisabarro, A.G., 2016. Comparative and transcriptional analysis of the predicted secretome in the lignocellulose-degrading basidiomycete fungus *Pleurotus ostreatus*. Environ. Microbiol. 18, 4710–4726.

Álvarez, J.M., Canessa, P., Mancilla, R.A., Polanco, R., Santibáñez, P.A., Vicuña, R., 2009. Expression of genes encoding laccase and manganese-dependent peroxidase in the fungus *Ceriporiopsis subvermispora* is mediated by an ACE1-like copper-fist transcription factor. Fungal Genet. Biol. 46, 104–111.

Amin, A.D., Vishnoi, N., Prochasson, P., 2012. A global requirement for the HIR complex in the assembly of chromatin. Biochim. Biophys. Acta. 1819, 264–276.

Antoniêto, A.C.C., dos Santos Castro, L., Silva-Rocha, R., Persinoti, G.F., Silva, R.N., 2014. Defining the genome-wide role of CRE1 during carbon catabolite repression in *Trichoderma reesei* using RNA-Seq analysis. Fungal Genet. Biol. 73, 93–103.

Avvakumov, N., Nourani, A., Côté, J., 2011. Histone chaperones: modulators of chromatin marks. Mol. Cell 41, 502–514.

Banumathy, G., Somaiah, N., Zhang, R., Tang, Y., Hoffmann, J., Andrake, M., Ceulemans, H., Schultz, D., Marmorstein, R., Adams, P.D., 2009. Human UBN1 is an ortholog of yeast Hpc2p and has an essential role in the HIRA/ASF1a chromatin-remodeling pathway in senescent cells. Mol. Cell Biol. 29, 58–770.

Bartholomew, K., Dos Santos, G., Dumonceaux, T., Charles, T., Archibald, F., 2001. Genetic transformation of *Trametes versicolor* to phleomycin resistance with the dominant selectable marker *shble*. Appl. Microbiol. Biotechnol. 56, 201–204.

Blackwell, C., Martin, K.A., Greenall, A., Pidoux, A., Allshire, R.C., Whitehall, S.K., 2004. The *Schizosaccharomyces pombe* HIRA-like protein Hip1 is required for the periodic expression of histone genes and contributes to the function of complex centromeres. Mol. Cell Biol. 24, 4309–4320.

Blanchette, R.A., 1991. Delignification by wood-decay fungi. Annu. Rev. Phytopathol. 29, 381–403.

Bok, J.W., Chiang, Y.M., Szewczyk, E., Reyes-Dominguez, Y., Davidson, A.D., Sanchez, J. F., Wang, C.C., 2009. Chromatin-level regulation of biosynthetic gene clusters. Nat. Chem. Biol. 5, 462.

Bonnefoy, E., Orsi, G.A., Couble, P., Loppin, B., 2007. The essential role of *Drosophila* HIRA for de novo assembly of paternal chromatin at fertilization. PLoS Genet. 3, e182.

Bugg, T.D., Ahmad, M., Hardiman, E.M., Rahmanpour, R., 2011. Pathways for degradation of lignin in bacteria and fungi. Nat. Prod. Rep. 28, 1883–1896.

Cragg, S.M., Beckham, G.T., Bruce, N.C., Bugg, T.D.H., Distel, D.L., Dupree, P., Etxabe, A. G., Goodel, B.S., Jellison, J., McGeehan, J.E., McQueen-Mason, S.J., Schnorr, K., Walton, P.H., Watts, J.E.M., Zimmer, M., 2015. Lignocellulose degradation mechanisms across the Tree of Life. Curr. Opn. Chem. Biol. 29, 108–119.

Derntl, C., Gudynaite-Savitch, L., Calixte, S., White, T., Mach, R.L., Mach-Aigner, A.R., 2013. Mutation of the Xylanase regulator 1 causes a glucose blind hydrolase expressing phenotype in industrially used *Trichoderma* strains. Biotechnol. Biofuels 6, 62.

DeSilva, H., Lee, K., Osley, M.A., 1998. Functional Dissection of Yeast HirAp, a WD Repeat-Containing Transcriptional Corepressor. Genetics 148, 657–667.

Dutta, D., Ray, S., Home, P., Saha, B., Wang, S., Sheibani, N., Tawfik, O., Cheng, N., Paul, S., 2010. Regulation of angiogenesis by histone chaperone HIRA-mediated incorporation of lysine 56-acetylated histone H3.3 at chromatin domains of endothelial genes. J. Biol. Chem. 285, 41567–41577.

Fernández-Fueyo, E., Ruiz-Dueñas, F.J., López-Lucendo, M.F., Pérez-Boada, M., Rencoret, J., Gutiérrez, A., Pisabarro, A.G., Ramírez, L., Martínez, A.T., 2016. A secretomic view of woody and nonwoody lignocellulose degradation by *Pleurotus ostreatus*. Biotechnol. Biofuels 9, 49.

Feldman, D., Kowbel, D.J., Glass, N.L., Yarden, O., Hadar, Y., 2017. A role for small secreted proteins (SSPs) in a saprophytic fungal lifestyle: Ligninolytic enzyme regulation in *Pleurotus ostreatus*. Sci. Rep. 7, 1–13.

Floudas, D., Binder, M., Riley, R., Barry, K., Blanchette, R.A., Henrissat, B., Martinez, A. T., Otillar, R., Spatafora, J.W., Yadav, J.S., Aerts, A., Benoit, I., Boyd, A., Carlson, A., Copeland, A., Coutinho, P.M., de Vries, R.P., Ferreira, P., Findley, K., Foster, B., Gaskell, J., Glotzer, D., Gorecki, P., Heitman, J., Hesse, C., Hori, C., Igarashi, K., Jurgens, J.A., Kallen, N., Kersten, P., Kohler, A., Kües, U., Kumar, T.K., Kuo, A., LaButti, K., Larrondo, L.F., Lindquist, E., Ling, A., Lombard, V., Lucas, S., Lundell, T., Martin, R., McLaughlin, D.J., Morgenstern, I., Morin, E., Murat, C., Nagy, L.G., Nolan, M., Ohm, R.A., Patyshakuliyeva, A., et al., 2012. The Paleozoic origin of enzymatic lignin decomposition reconstructed from 31 fungal genomes. Science 336, 1715–1719.

Green, J.W., 1963. Wood cellulose. In: Whistler, R.L. (Ed.), Methods in Carbohydrate Chemistry, 3. Academic Press USA, pp. 9–21.

Greenall, A., Williams, E.S., Martin, K.A., Palmer, J.M., Gray, J., Liu, C., Whitehall, S.K., 2006. Hip3 interacts with the HIRA proteins Hip1 and Slm9 and is required for transcriptional silencing and accurate chromosome segregation. J. Biol. Chem. 281, 8732–8739.

Hori, C., Gaskell, J., Igarashi, K., Kersten, P., Mozuch, M., Samejima, M., Cullen, D., 2014. Temporal alterations in the secretome of the selective ligninolytic fungus *Ceriporiopsis subvermispora* during growth on aspen wood reveal this organism's strategy for degrading lignocellulose. Appl. Environ. Microbiol. 80, 2062–2070.

Honda, Y., Matsuyama, T., Irie, T., Watanabe, T., Kuwahara, M., 2000. Carboxin resistance transformation of the homobasidiomycete fungus *Pleurotus ostreatus*. Curr. Genet. 37, 209–212.

Hu, Y., Xu, W., Hu, S., Lian, L., Zhu, J., Shi, L., Ren, A., Zhao, M., 2020. In *Ganoderma lucidum*, Glsnf1 regulates cellulose degradation by inhibiting GlCreA during the utilization of cellulose. Environ. Microbiol. 22, 107–121.

Inada, K., Morimoto, Y., Arima, T., Murata, Y., Kamada, T., 2001. The *clp1* gene of the mushroom *Coprinus cinereus* is essential for *A*-regulated sexual development. Genetics 157, 133–140.

Kamitsuji, H., Honda, Y., Watanabe, T., Kuwahara, M., 2004. Production and induction of manganese peroxidase isozymes in a white-rot fungus *Pleurotus ostreatus*. Appl. Microbiol. Biotechnol. 65, 287–294.

König, J., Grasser, R., Pikor, H., Vogel, K., 2002. Determination of xylanase, β-glucanase, and cellulase activity. Anal. Bioanal. Chem. 374, 80–87.

Larraya, L.M., Pérez, G. Penas M.M., Baars, J.J., Mikosch, T.S., Pisabarro, A.G., Ramírez L., 1999. Molecular karyotype of the white rot fungus Pleurotus ostreatus. Appl. Environ. Microbiol. 65, 3413–3417.

Li, Y., Jiao, J., 2017. Histone chaperone HIRA regulates neural progenitor cell proliferation and neurogenesis via β-catenin. J. Cell Biol. 216, 1975–1992.

Lombard, V., Golaconda Ramulu, H., Drula, E., Coutinho, P.M., Henrissat, B., 2013. The carbohydrate-active enzymes database (CAZy) in 2013. Nucleic Acids Res. 42, D490–D495.

Loppin, B., Bonnefoy, E., Anselme, C., Laurençon, A., Karr, T.L., Couble, P., 2005. The histone H3. 3 chaperone HIRA is essential for chromatin assembly in the male pronucleus. Nature 437, 1386–1390.

Lundell, T.K., Mäkelä, M.R., Hildén, K., 2010. Lignin-modifying enzymes in filamentous basidiomycetes–ecological, functional and phylogenetic review. J. Basic Microbiol. 50, 5–20.

Manavalan, T., Manavalan, A., Heese, K., 2015. Characterization of lignocellulolytic enzymes from white-rot fungi. Curr. Microbiol. 70, 485–498.

Marfella, C.G., Imbalzano, A.N., 2007. The Chd family of chromatin remodelers. Mutat. Res.-Fund. Mol. M. 618, 30–40.

Martinez, D., Challacombe, J., Morgenstern, I., Hibbett, D., Schmoll, M., Kubicek, C.P., Ferreira, P., Ruiz-Duenas, F.J., Martinez, A.T., Kersten, P., Hammel, K.E., Vanden Wymelenberg, A., Gaskell, J., Lindquist, E., Sabat, G., Splinter BonDurant, S., Larrondo, L.F., Canessa, P., Vicuna, R., Yadav, J., Doddapaneni, H., Subramanian, V., Pisabarro, A.G., Lavin, J.L., Oguiza, J.A., Master, E., Henrissat, B., Coutinho, P.M., Harris, P., Magnuson, J.K., Baker, S.E., Bruno, K., Kenealy, W., Hoegger, P.J., Kües, U., Ramaiya, P., Lucas, S., Salamov, A., Shapiro, H., Tu, H., Chee, C.L., Misra, M., Xie, G., Teter, S., Yaver, D., James, T., Mokrejs, M., Pospisek, M., Grigoriev, I.V., Brettin, T., et al., 2009. Genome, transcriptome, and secretome analysis of wood decay fungus *Postia placenta* supports unique mechanisms of lignocellulose conversion. Proc. Natl. Acad. Sci. 106, 1954–1959.

Matsunaga, Y., Ando, M., Izumitsu, K., Suzuki, K., Honda, Y., Irie, T., 2017. A development and an improvement of selectable markers in *Pleurotus ostreatus* transformation. J. Microbiol. Meth. 134, 27–29.

Mello-de-Sousa, T.M., Rassinger, A., Derntl, C., J Poças-Fonseca, M., L Mach, R., R Mach-Aigner, A., 2016. The relation between promoter chromatin status, Xyr1 and cellulase expression in Trichoderma reesei. Curr. Genomics 17, 145–152.

Mizuki, F., Tanaka, A., Hirose, Y., Ohkuma, Y., 2011. The HIRA complex subunit Hip3 plays important roles in the silencing of meiosis-specific genes in *Schizosaccharomyces pombe*. PLoS ONE 6, e19442.

Muraguchi, H., Ito, Y., Kamada, T., Yanagi, S.O., 2003. A linkage map of the basidiomycete *Coprinus cinereus* based on random amplified polymorphic DNAs and restriction fragment length polymorphisms. Fungal Genet. Biol. 40, 93–102.

Nakazawa, T., Kaneko, S., Miyazaki, Y., Jojima, T., Yamazaki, T., Katsukawa, S., Shishido, K., 2008. Basidiomycete *Lentinula edodes* CDC5 and a novel interacting protein CIPB bind to a newly isolated target gene in an unusual manner. Fungal Genet. Biol. 45, 818–828.

Nakazawa, T., Honda, Y., 2015. Absence of a gene encoding cytosine deaminase in the genome of the agaricomycete *Coprinopsis cinerea* enables simple marker recycling through 5-Fluorocytosine counter-selection. FEMS Microbiol. Lett. 362, fnv123.

Nakazawa, T., Tsuzuki, M., Irie, T., Sakamoto, M., Honda, Y., 2016. Marker recycling via 5-fluoroorotic acid and 5-fluorocytosine counter-selection in the white-rot agaricomycete *Pleurotus ostreatus*. Fungal Biol. 120, 1146–1155.

Nakazawa, T., Izuno, A., Kodera, R., Miyazaki, Y., Sakamoto, M., Isagi, Y., Honda, Y., 2017a. Identification of two mutations that cause defects in the ligninolytic system through efficient forward genetics in the white-rot agaricomycete *Pleurotus ostreatus*. Environ. Microbiol. 19, 261–272.

Nakazawa, T., Izuno, A., Horii, M., Kodera, R., Nishimura, H., Hirayama, Y., Tsunematsu, Y., Miyazaki, Y., Awano, T., Muraguchi, H., Watanabe, K., Sakamoto, M., Takabe, K., Watanabe, T., Isagi, Y., Honda, Y., 2017b. Effects of *pex1* disruption on wood lignin biodegradation, fruiting development and the utilization of carbon sources in the white-rot Agaricomycete *Pleurotus ostreatus* and non-wood decaying *Coprinopsis cinerea*. Fungal Genet. Biol. 109, 7–15.

Nakazawa, T., Morimoto, R., Wu, H., Kodera, R., Sakamoto, M., Honda, Y., 2019. Dominant effects of *gat1* mutations on the ligninolytic activity of the white-rot fungus *Pleurotus ostreatus*. Fungal Biol. 123, 209–217.

Nguyen, D.X., Sakaguchi, T., Nakazawa, T., Sakamoto, M., Honda, Y., 2020. A 14-bp stretch plays a critical role in regulating gene expression from β 1-tubulin promoters of basidiomycetes. Curr. Genet. 66, 217–228.

Pham, K.T.M., Inoue, Y., Van Vu, B., Nguyen, H.H., Nakayashiki, T., Ikeda, K.I., Nakayashiki, H., 2015. MoSET1 (histone H3K4 methyltransferase in *Magnaporthe oryzae*) regulates global gene expression during infection-related morphogenesis. PLoS Genet. 11, e1005385.

Portnoy, T., Margeot, A., Linke, R., Atanasova, L., Fekete, E., Sándor, E., Hartl, L., Karaffa, L., Druzhinina, I.S., Seiboth, B., Le Crom, S., Kubicek, C.P., 2011. The CRE1 carbon catabolite repressor of the fungus *Trichoderma reesei*: a master regulator of carbon assimilation. BMC Genomics 12, 269.

Radman-Livaja, M., Quan, T.K., Valenzuela, L., Armstrong, J.A., Van Welsem, T., Kim, T., Lee, L.J., Buratowski, S., van Leeuwen, F., Rando, O.J., Hartzog, G.A., 2012. A key role for Chd1 in histone H3 dynamics at the 3′ ends of long genes in yeast. PLoS Genet. 8, e1002811.

Rai, T.S., Puri, A., McBryan, T., Hoffman, J., Tang, Y., Pchelintsev, N.A., van Tuyn, J., Marmorstein, R., Schultz, D.C., Adams, P.D., 2011. Human CABIN1 is a functional member of the human HIRA/UBN1/ASF1a histone H3. 3 chaperone complex. Mol. Cell Biol. 31, 4107–4118.

Rao, P.S., Niederpruem, D.J., 1969. Carbohydrate metabolism during morphogenesis of *Coprinus lagopus* (sensu Buller). J. Bacteriol. 100, 1222–1228.

Ricketts, M.D., Marmorstein, R., 2017. A molecular prospective for HIRA complex assembly and H3. 3-specific histone chaperone function. J. Mol. Biol. 429, 1924–1933.

Ritter, G.J., Seborg, R.M., Mitchell, R.L., 1932. Factors affecting quantitative determination of lignin by 72 per cent sulfuric acid method. Ind. Eng. Chem. Anal. Ed. 4, 202–1024.

Rytioja, J., Hildén, K., Yuzon, J., Hatakka, A., de Vries, R.P., Mäkelä, M.R., 2014. Plant-polysaccharide-degrading enzymes from basidiomycetes. Microbiol. Mol. Biol. Rev. 78, 614–649.

Rytioja, J., Hildén, K., Di Falco, M., Zhou, M., Aguilar-Pontes, M.V., Sietiö, O.M., Tsang, A., de Vries, R.P., Mäkelä, M.R., 2017. The molecular response of the white-rot fungus *Dichomitus squalens* to wood and non-woody biomass as examined by transcriptome and exoproteome analyses. Environ. Microbiol. 19, 1237–1250.

Salame, T.M., Yarden, O., Hadar, Y., 2010. *Pleurotus ostreatus* manganese-dependent peroxidase silencing impairs decolourization of Orange II. Microb. Biotechnol. 3, 93–106.

Salame, T.M., Knop, D., Tal, D., Levinson, D., Yarden, O., Hadar, Y., 2012. Predominance of a versatile-peroxidase-encoding gene, *mnp4*, as demonstrated by gene replacement via a gene targeting system for *Pleurotus ostreatus*. Appl. Environ. Microbiol. 78, 5341–5352.

Salame, T.M., Knop, D., Levinson, D., Yarden, O., Hadar, Y., 2013. Redundancy among manganese peroxidase in *Pleurotus ostreatus*. Appl. Environ. Microbiol. 79, 2405–2415.

Salame, T.M., Knop, D., Levinson, D., Mabjeesh, S.J., Yarden, O., Hadar, Y., 2014. Inactivation of a *Pleurotus ostreatus* versatile peroxidase-encoding gene (*mnp2*) results in reduced lignin degradation. Environ. Microbiol. 16, 265–277.

Sánchez, C., 2009. Lignocellulosic residues: biodegradation and bioconversion by fungi. Biotechnol. Adv. 27, 185–194.
Sharma, K.K., Gupta, S., Kuhad, R.C., 2006. Agrobacterium-mediated delivery of marker genes to *Phanerochaete chrysosporium* mycelial pellets: a model transformation system for white-rot fungi. Biotechnol. Appl. Biochem. 43, 181–186.
Sherwood, P.W., Tsang, S.V., Osley, M.A., 1993. Characterization of HIRA and HIR2, two genes required for regulation of histone gene transcription in *Saccharomyces cerevisiae*. Mol. Cell Biol. 13, 28–38.
Strauss, J., Mach, R.L., Zeilinger, S., Hartler, G., Stöffler, G., Wolschek, M., Kubicek, C.P., 1995. Crel, the carbon catabolite repressor protein from *Trichoderma reesei*. FEBS Lett. 376, 103–107.
Tagami, H., Ray-Gallet, D., Almouzni, G., Nakatani, Y., 2004. Histone H3. 1 and H3. 3 complexes mediate nucleosome assembly pathways dependent or independent of DNA synthesis. Cell 116, 51–61.
Toyokawa, C., Shobu, M., Tsukamoto, R., Okamura, S., Honda, Y., Kamitsuji, H., Izumitsu, K., Suzuki, K., Irie, T., 2016. Effects of overexpression of PKAc genes on expressions of lignin-modifying enzymes by *Pleurotus ostreatus*. Biosci. Biotechnol. Biochem. 80, 1759–1767.
Tsukamoto, A., Kojima, Y., Kita, Y., Sugiura, J., 2003. Transformation of the white-rot basidiomycete *Coriolus hirsutus* using the ornithine carbamoyltransferase gene. Biosci. Biotenol. Biochem. 67, 2075–2082.
van Peij, N.N., Gielkens, M.M., de Vries, R.P., Visser, J., de Graaff, L.H., 1998. The transcriptional activator XlnR regulates both xylanolytic and endoglucanase gene expression in *Aspergillus niger*. Appl. Microbiol. Biol. 64, 3615–3619.
Vyas, B.R., Molitoris, H.P., 1995. Involvement of an extracellular H_2O_2-dependent ligninolytic activity of the white rot fungus *Pleurotus ostreatus* in the decolorization of Remazol brilliant blue R. Appl. Environ. Microbiol. 61, 3919–3927.
Wei, H., Xu, Q., Taylor II, L.E., Baker, J.O., Tucker, M.P., Ding, S.Y., 2009. Natural paradigms of plant cell wall degradation. Curr. Opin. Biotechnol. 20, 330–338.
Wu, H., Nakazawa, T., Takenaka, A., Kodera, R., Morimoto, R., Sakamoto, M., Honda, Y., 2020. Transcriptional shifts in delignification-defective mutants of the white-rot fungus *Pleurotus ostreatus*. FEBS Lett. 594, 3182–3199.
Xin, Q., Gong, Y., Lv, X., Chen, G., Liu, W., 2013. *Trichoderma reesei* histone acetyltransferase Gcn5 regulates fungal growth conidiation and cellulase gene expression. Curr. Microbiol. 67, 580–589.
Yasuno, S., Murata, T., Kokubo, K., Yamaguchi, T., Kamei, M., 1997. Two-mode analysis by High-performance liquid chromatography of *p*-Aminobenzoic ethyl ester-derivatized monosaccharides. Biosci. Biotechnol. Biochem. 61, 1944–1946.
Yoav, S., Salame, T.M., Feldman, D., Levinson, D., Ioelovich, M., Morag, E., Yarden, O., Bayer, E.A., Hadar, Y., 2018. Effects of *cre1* modification in the white-rot fungus *Pleurotus ostreatus* PC9: altering substrate preference during biological pretreatment. Biotechnol. Biofuels 11, 212.
Zhang, J., Silverstein, K.A., Castaño, J.D., Figueroa, M., Schilling, J.S., 2019. Gene Regulation Shifts Shed Light on Fungal Adaption in Plant Biomass Decomposers. mBio 10, e02176–e2219.
Zolan, M.E., Pukkila, P.J., 1986. Inheritance of DNA methylation in *Coprinus cinereus*. Mol. Cell Biol. 6, 195–200.